Applied Catalysis B: Environmental 188 (2016) 154–168

Contents lists available at ScienceDirect

Applied Catalysis B: Environmental

journal homepage: www.elsevier.com/locate/apcatb

Gold catalysts supported on Y-modified ceria for CO-free hydrogen production *via* PROX

L. Ilieva[a,*], P. Petrova[a], G. Pantaleo[b,**], R. Zanella[c], L.F. Liotta[b], V. Georgiev[a], S. Boghosian[d], Z. Kaszkur[e], J.W. Sobczak[e], W. Lisowski[e], A.M. Venezia[b], T. Tabakova[a]

[a] *Institute of Catalysis, Bulgarian Academy of Sciences, 1113 Sofia, Bulgaria*
[b] *Istituto per lo Studio di Materiali Nanostrutturati, CNR, I-90146 Palermo, Italy*
[c] *Centro de Ciencias Aplicadas y Desarrollo TeGcnológico, Universidad Nacional Autónoma de México, Circuito Exterior S/N, Ciudad Universitaria, C. P. 04510 México D.F., Mexico*
[d] *Department of Chemical Engineering, University of Patras and FORTH/ICE-HT, Patras, Greece*
[e] *Institute of Physical Chemistry, PAS, Kasprzaka 44/52, 01-224 Warsaw, Poland*

ARTICLE INFO

Article history:
Received 17 November 2015
Received in revised form 27 January 2016
Accepted 1 February 2016
Available online 3 February 2016

Keywords:
Gold catalysts
Y-doped ceria
Preparation method
PROX

ABSTRACT

The preferential CO oxidation in the presence of excess hydrogen (PROX) was studied over gold catalysts on yttrium-modified ceria supports synthesized by impregnation (IM) and co-precipitation (CP) methods. In order to avoid oxygen vacancies ordering by heavily yttrium doping, a low extent Y-modification of ceria (up to 7.5 wt.% Y_2O_3, *i.e.*, 11 at.% Y) was investigated. The samples were characterized by XRD, HRTEM/HAADF, Raman and XP spectroscopy and TPR measurements. At the operating temperature of the fuel cells (80–120 °C) the selectivity of the Y-doped gold catalysts was larger than that of Au/CeO_2. However, at these temperatures all studied catalysts exhibited quite similar PROX activity and selectivity. This was explained by the similarity in relatively small average size of gold particles (estimated by HRTEM in the 2.1–3.5 nm range) and the reducibility of ceria surface layers. Raman spectroscopy showed a higher extent of bulk defects, O vacancies and interstitials with increasing Y-doping in the supports made by the CP method and-based on sequential spectra obtained under oxidizing and reducing conditions- enabled the assignment of a band at ~605 cm^{-1} to a vibrational mode within the anionic (oxygen) sub-lattice that involve mobile (detachable) oxygen atoms that can be delivered by the support under suitable conditions. The absence of correlation between CO conversion and yttrium loading could suggest a preferential role played by the surface modification and surface oxygen mobility in PROX. Although under ideal conditions there was not substantial dependence of the behavior in PROX on the preparation method of doped supports, the IM method was more appropriate than the CP method for PROX with CO_2 and water addition to the gas feed. The improved tolerance to CO_2 could be explained by the lowering of ceria surface basicity due to the nanosized Y_2O_3, covering ceria grains.

1. Introduction

Hydrogen utilization in the proton exchange membrane (PEM) fuel cells to transform the chemical energy into electricity with zero harmful emissions is a topical issue. Hydrogen is mainly produced by hydrocarbons (from fossil or from renewable sources) reforming followed by water gas shift reaction (WGSR) to enhance the production of H_2 and lower the CO concentration in the reformate stream down to 1–2%. However, to prevent the poisoning of fuel cell anodes, the CO amount must be below 10 ppm for Pt anodes and below 100 ppm for CO-tolerant alloy anodes. One of the most effective and economic ways for CO cleanup is its preferential oxidation in the presence of excess hydrogen (PROX). The key issues for PROX catalysts are: (i) control of the undesirable hydrogen oxidation reaction; (ii) in order to avoid the heat changes, the temperature range of high catalytic activity and selectivity in PROX must be the fuel cells operating temperature interval 80–120 °C. This is in line with the catalytic behavior of oxide-supported gold catalysts, exhibiting a satisfactory balance of high activity and selectivity at relatively low temperatures due to the lower energy barrier for CO oxidation as compared to H_2 oxidation [1]. A recent survey [2 and

* Corresponding author at: Institute of Catalysis, Bulgarian Academy of Sciences, Acad. G. Bonchev St., Block 11, 1113 Sofia, Bulgaria.
** Corresponding author.
E-mail addresses: luilieva@ic.bas.bg (L. Ilieva), pantaleo@pa.ismn.cnr.it (G. Pantaleo).

http://dx.doi.org/10.1016/j.apcatb.2016.02.004
0926-3373/

references therein] has been focused on the developments of gold-based PROX catalysts and reviewed the effects of the nature of the support (composition, size and morphology), the influence of promoters and the characteristics of gold on the catalytic performance in PROX. Other aspects of the catalysts' behavior in performance grounds, such as (i) high CO conversion with excellent selectivity toward CO_2, (ii) good resistance against the effects of H_2O and CO_2 (in the real reaction stream the usual CO_2 concentration is about 20% and the H_2O amount is about 10%), (iii) stable and reproducible catalytic behavior are far from being well understood. To this end, studies of nanosized gold catalysts for CO-free hydrogen production are of high priority and relevance.

Ceria is an appropriate support for gold catalysts in PROX [3–6] due to its well-known high oxygen storage capacity (OSC). Besides, the intimate interaction between gold and ceria leads to small gold particles stabilization. Doping foreign cations into the ceria lattice is known to improve the redox properties of ceria because of the induced structural and electronic changes. The use of different dopants and various preparation methods could influence not only the OSC of ceria-based supports but the gold dispersion as well.

PROX over gold catalysts on ceria modified with rare earths was investigated in several studies [7–9]. In a recent study by Ilieva et al. [10] praseodymium was chosen as a modifier of ceria. The own redox behavior ($Pr^{4+} \leftrightarrow Pr^{3+}$) was expected to enhance the oxygen supplying by the support. However, a lower CO conversion of gold catalysts on Pr-doped with respect to the undoped ceria was established and the results were attributed to the Pr presence, hindering the surface re-oxidation. The efforts for selection of ceria based gold catalysts with high activity, CO_2 selectivity and long-term stability in PROX at real feed conditions (presence of CO_2 and water) continue in the present study using yttrium as ceria modifier. The yttrium supply is abundant and the Y-doped CeO_2 systems encountered a special interest among doped CeO_2 materials. In a previous study it has been shown that the gold catalyst on Y-modified ceria, prepared by co-precipitation, exhibited the highest PROX activity and selectivity as compared to gold catalysts supported on ceria modified by other rare earths as La, Sm and Gd [9]. However, the results obtained by Jardim et al. [11] pointed out that the Y doping of ceria did not improve the PROX activity and the stability of the gold catalyst, which was less resistant to the thermal treatment as compared to gold on bare ceria. The explanation was related to the large dopant segregation at the surface, leading to higher mobility and sintering of the gold nanoparticles, because the study was carried out with high amount of Y-doping (30 wt.% Y_2O_3). The review of the literature leads to the conclusion that the oxygen ion conductivity (related to OSC) is a function of dopant concentration and that heavily yttrium doped ceria (*i.e.*, above 10–15 at.% [12–14 and references therein]) causes its lowering because of oxygen vacancy ordering. Atribak et al. [15] have studied $Ce_{1-x}Y_xO_2$ catalysts for soot oxidation in air and they concluded that the high yttrium loading ($x = 0.12$) is less effective than low dosage ($x = 0.01$). The results obtained by She et al. revealed that catalytic activity in WGSR first increased with increasing Y amount, but then decreased with further increase in the Y content; CuO/CeO_2 catalyst doped with 2 wt.% of Y_2O_3 showed the highest catalytic activity and thermal stability [16].

The motivation for studying gold catalysts supported on Y_2O_3-doped CeO_2 at low/moderate extent of Y-doping for CO—free hydrogen production *via* PROX comes as straightforward consequence of the aforementioned results. The effect of various Y amounts and different support preparation methods on the gold particles size and supports features was studied by means of XRD, HRTEM/HAADF, high temperature Raman and XP spectroscopy and TPR measurements. The impact of moisture and CO_2 on the catalytic activity and selectivity in PROX over selected catalysts was examined as well.

2. Experimental

2.1. Sample preparation

Two series of yttrium-modified ceria supports were prepared by impregnation (IM) and by co-precipitation (CP) methods. Different Y-dopant amounts were chosen: 1, 2.5, 5 and 7.5 wt.% of Y_2O_3 or correspondingly 1.5, 3.8, 7.4 and 11.0 at.% of Y. Aqueous solutions of $Y(NO_3)_3{\cdot}6H_2O$ were used for the impregnation of ceria that was carried out by vigorous stirring at room temperature for 4 h. Then, the suspension was evaporated under vacuum at 70 °C in a rotary evaporator until water was completely removed. Ceria was prepared by precipitation of aqueous solution of $Ce(NO_3)_3{\cdot}6H_2O$ with K_2CO_3 at constant pH = 9.0 and at a temperature of 60 °C. Using the second technique (CP), the supports were prepared from a solution of the corresponding Y and Ce nitrates in appropriate ratio, coprecipitated with a solution of K_2CO_3 at constant pH 9.0 and temperature 60 °C. The precipitates were aged at the same temperature for 1 h, then filtered and washed until removal of NO_3^- ions. All resulting precursors were dried in vacuum at 80 °C and calcined in air at 400 °C for 2 h. The mixed supports were denoted as *x*YCeIM and *x*YCeCP, correspondingly ($x = 1$, 2.5, 5 and 7.5, denoting the wt.% amount of Y_2O_3).

Gold (3 wt.%) was loaded by the deposition-precipitation method. It was deposited onto mixed oxides thoroughly suspended in water *via* chemical interaction between $HAuCl_4{\cdot}3H_2O$ and K_2CO_3, under vigorous stirring, while keeping constant pH = 7.0. The precipitation was carried out using the 'Contalab' system (Switzerland) under full control of all parameters of preparation (pH, temperature, stirring speed, reactant feed flow rates, etc.). After filtering and careful washing, the precursors were dried under vacuum and calcined in air at 400 °C for 2 h. A careful inspection of XP spectra of the gold catalysts showed that no peaks related to the Cl presence were registered. The gold-containing samples were denoted as Au*x*YCeIM and Au*x*YCeCP, correspondingly.

All the initial salts used were "analytical grade".

2.2. Sample characterization

The BET surface area (S_{BET}) of the samples was determined on a Carlo Erba Sorptomat 1900 instrument. The fully computerized analysis of the nitrogen adsorption isotherm at −196 °C allowed estimating the specific surface areas of the samples in the standard pressure range 0.05–0.3 p/p_o. Prior to the measurements, the samples were outgassed at 200 °C for 30 min under vacuum.

The actual gold loading for each catalyst was 3 (±0.05) wt%, as measured by Atomic Absorption spectroscopy using Varian Vista MPX apparatus.

X-ray powder diffraction (XRD) measurements were performed using aD5000 diffractometer (Bruker AXS), with Cu sealed tube operating at 40 kV and 40 mA. The setup employed Bragg-Brentano focusing geometry with 1 deg. beam divergence and LynxEye strip detector. The data were analyzed using PeakFit program (Jandel Scientific) fitting XRD profiles to Kα 1,2 doublets having PEARSON VII analytical form. The crystal size of gold particles was estimated from FWHM (full width at half maximum) of the strongest (1 1 1) reflection. The CeO_2 phase was analyzed on the basis of 14 well measured reflections and Williamson-Hall plot [17,18] and the average crystal size (average column length over all available crystallographic directions) was calculated.

High resolution transmission electron microscopy (HRTEM) and high angle annular dark field (HAADF) observations of the gold

catalysts were performed in a JEM 2010 FasTem analytical microscope equipped with a Z-contrast annular detector. The histograms of the gold particle sizes were established from the measurement of more than 2000 particles obtained by Z-contrast observations.The mean particle size (D_s) of gold was calculated using the formula $D_s = \sum n_i D_i / \sum n_i$ where n_i is the number of particles of diameter D_i.

The X-ray photoelectron (XP) spectra were registered on a PHI 5000 VersaProbe scanning ESCA Microprobe using monochromatic Al- Kα radiation ($h\nu$=1486.6 eV) from an X-ray source operating at 200 μm spot size, 50 W and 15 kV. The analyzer pass energy was 23.5 eV, an electron take-off angle was 80° and the energy step size was 0.1 eV. The samples were pressed into thin wafers and degassed in a preparation chamber before analysis. The Shirley background subtraction and peak fitting with Gaussian–Lorentzian product peak was performed using a CasaXPS processing program. The charging effects were corrected by adjusting the Ce $3d_{3/2}$ peak, usually described as the u‴ peak, to a position of 917.00 eV [19–21].

Raman spectra were excited with the 491.5 nm blue line of a Diode Pumped Solid State laser (Cobolt, Sweden) operated typically at a power level of 40 mW (measured before the focusing cylindrical lens); the incident laser light was slightly defocused in order to reduce sample irradiance. The right angle scattered light (at a horizontal scattering plane/90° scattering geometry) was analyzed by a Spex 1403, 0.85 m double monochromator, and detected with a −20 °C cooled RCA photomultiplier tube interfaced with a Labspec (JobinYvon) data acquisition software. The resolution was set at 7 cm^{-1}. A home made *in situ* Raman cell was used for recording the Raman spectra at high temperature under controlled gas atmosphere [22]. The sample supporter used can accommodate a pressed wafer disc for recording spectra of powdered catalyst samples. The Raman spectra were recorded for all *x*YCeIM and *x*YCeCP mixed supports under flowing 20% O_2 gas (balance He) at 200 °C after subjecting each sample to the same conditions in the *in situ* Raman cell for 1 h. The Raman cell, as well as the procedures followed for recording Raman spectra of catalyst samples were recently described elsewhere [22]. The redox behavior of the mixed supports was furthermore studied by recording *sequential in situ* Raman spectra at 480 °C under flowing 20% O_2/He and (subsequently) under 5% H_2/He gas after adequately subjecting the samples to each gas mixture (*i.e.*, for 1 h under 20% O_2/He and 2 h under 5% H_2/He). The reinstatement of each studied sample in its initial oxidized state was verified by re-subjecting the sample to oxidizing conditions and recording the *in situ* Raman spectrum under flowing 20%/O_2/He at 480 °C.

The temperature programmed reduction (TPR) measurements were carried out by means of an apparatus described elsewhere [23]. A cooling trap (−40 °C) for removing water formed during reduction was mounted in the gas line prior to the thermal conductivity detector. A hydrogen-argon mixture (10% H_2), dried over a molecular sieve 5A (−40 °C), was used to reduce the samples at a flow rate of 24 mL min^{-1}. The temperature was linearly raised at a rate of 15 °C min^{-1}. The amount of sample used was 0.05 g, based on a criterion proposed by Monti and Baiker [24]. The hydrogen consumption during the TPR measurements was calculated using preliminary calibration of the thermal conductivity detector, performed by reducing of different amounts of NiO to Ni°. NiO was 'analytical grade', calcined at 800 °C for 2 h to avoid the presence of non-stoichiometric oxygen.

2.3. Catalytic measurements

The measurements of the catalytic activity in PROX, expressed as degree of CO conversion and selectivity toward CO_2, were carried out in the temperature range 40–180 °C using a quartz glass U-shaped reactor, equipped with a temperature programmed controller. The amount of tested catalyst was 0.05 g. The total gas feed rate was 50 mL min^{-1}, containing 60% H_2 + 1% CO + 1% O_2 and He as balance (WHSV of 60 000 mL g^{-1} h^{-1}). On the basis of preliminary tests following catalyst pretreatment in oxidizing or reductive atmosphere, the treatment before the catalytic tests was chosen using 5% H_2 in He for 30 min at 150 °C.

The CO conversion and the selectivity were calculated using an ABB infrared analyzer detector for CO and CO_2 and an ABB paramagnetic Magnos206 for the O_2. The converted CO was calculated on the basis of the CO_2 produced whereas the selectivity was estimated according to the following equation:

$$S = \frac{ppmCO_2{}^{out}}{2 \times (ppmO_2{}^{in} - ppmO_2{}^{out})} \times 100\ (in\ \%)$$

The catalytic test over selected catalysts was also carried out using a gas feed composition of 50% H_2 + 1% CO + 1% O_2 + 10% CO_2 + 10% H_2O and He as balance (50% H_2 was used in order to keep the same total gas inlet of 50 mL min^{-1}).

3. Results

3.1. Catalytic activity and selectivity in PROX

Fig. 1 shows the comparison between CO conversion (A and B) and selectivity (C and D) in PROX over the studied gold catalysts on lightly Y-doped ceria supports prepared by IM and CP, respectively. In all cases 100% O_2 conversion was reached at 80 °C and above. Methane formation was not detected for any of the studied catalysts. At low temperature (LT) of around 40 °C, the activity of gold catalysts on IM supports is notably higher (85–90% CO conversion, except that of 65% in the case of 7.5 wt.% dopant), when compared to the corresponding catalysts on CP supports (64–70% CO conversion); the CO conversion of AuCe sample is the lowest one. In the range of interest for PROX, *i.e.*, at 80 °C the CO conversion was 78–82% for all the yttrium doped gold catalysts; a lower conversion was observed at 120 °C. The highest selectivity toward CO_2 in this range was measured for Au2.5YCeIM (45% at 80 °C and 41% at 120 °C), which compared favorably with the lowest value observed for the undoped AuCe (33% at 80 °C and 31% at 120 °C).

The catalysts, containing 2.5 wt.% dopant, were tested under more realistic conditions by adding CO_2 and water to the feed gas stream (Fig. 2). A drop of CO conversion was observed for both the CP and the IM support prepared catalysts, to a much larger extent for CP one.

3.2. Catalysts characterization

Table 1 lists the specific surface area (S_{BET}) of the studied gold catalysts. A decrease of S_{BET} is observed with increasing dopant amount for both routes of synthesis. There is a tendency for slightly lower surface for the Au*x*YCeIM catalysts. The XRD patterns of gold catalysts on Y-doped ceria prepared by IM (A) and CP (B) are illustrated in Fig. 3. The gold signals were very weak and the only visible reflections of metallic Au (1 1 1) were that at $2\theta = 38.2°$. Reflections typical for cubic fluorite-type structure of CeO_2 and no diffraction lines of segregated Y_2O_3 phase were detected. From the analysis of the diffraction patterns, the average size of gold particles and that of ceria crystallites, as well as ceria lattice constant (a) were calculated and listed in Table 1. The size of gold particles does not depend on the preparation method and there is no significant difference in ceria average particle size and cell parameter among the samples.

In order to determine the size distribution of gold a careful analysis of HRTEM and Z contrast (HAADF) images was carried out. Fig. 4 shows the HRTEM and the HAADF images of Au2.5YCeIM

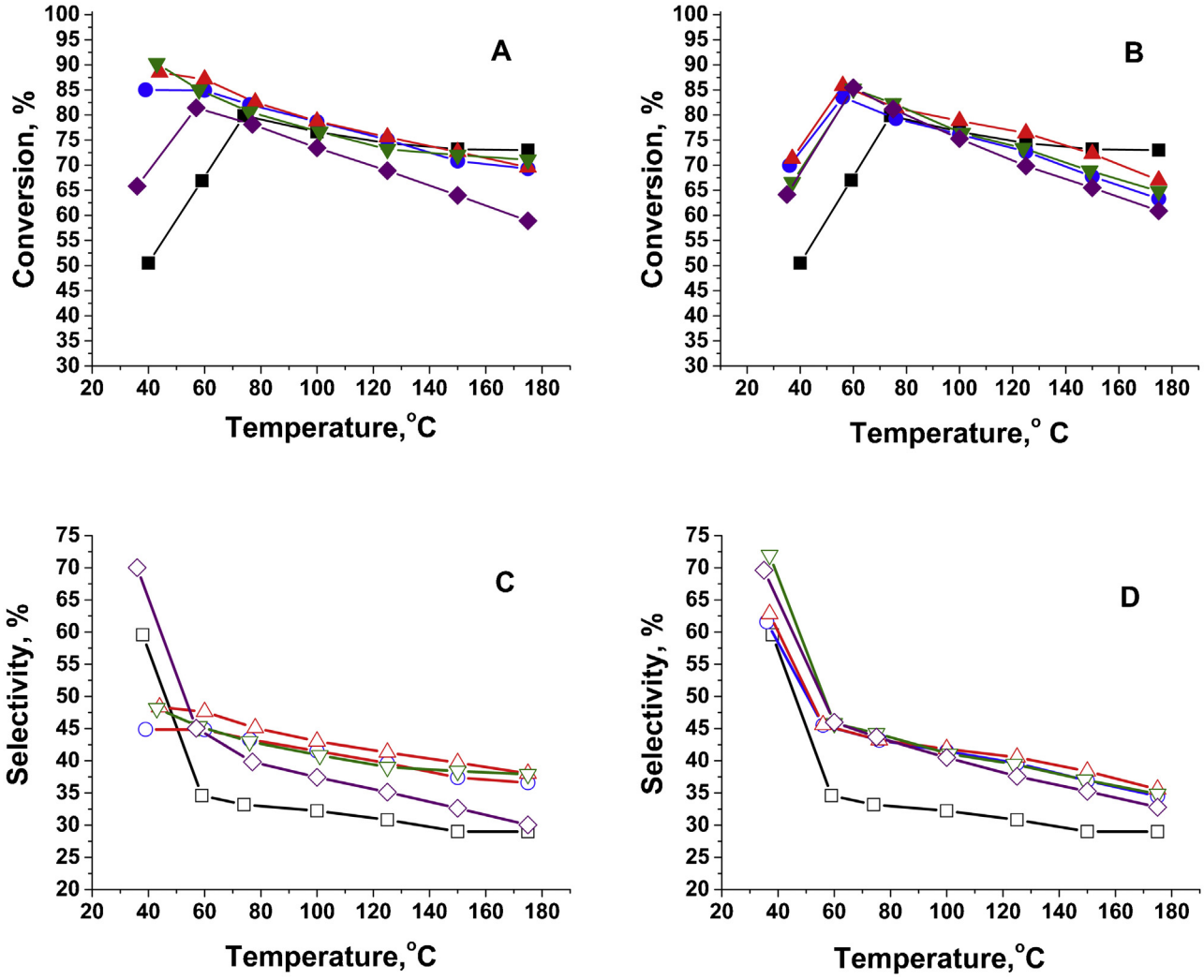

Fig. 1. (A) CO conversion and (C) selectivity of gold catalysts on supports prepared by IM; (B) CO conversion and (D) selectivity of gold catalysts on supports prepared by CP, where for conversion are used filled symbols: (-■-)—AuCe, (-●-)—Au1YCe, (-▲-)—Au2.5YCe, (-▼-)—Au5YCe, (-♦-)—Au7.5YCe, and empty ones for selectivity: (-□-)—AuCe, (-○-)—Au1YCe, (-Δ-)—Au2.5YCe, (-▽-)—Au5YCe and (-◊-)—Au7.5YCe.

Table 1
BET surface area (S_{BET}), lattice constant of ceria (a), average size of ceria and gold particles, estimated by XRD and HRTEM/HAADF.

Sample	S_{BET} ($m^2\ g^{-1}$)	a_{XRD} (nm)	$D_{XRD}(CeO_2)$ (nm)	D_{XRD}(Au) (nm)	D_{HRTEM}(Au) (nm)
AuCe	102.4	0.5413(1)*	5.7(1)*	5.7	2.1
Au1YCeIM	87.2	0.5415(2)	7.1(6)	2.9	2.6
Au2.5YCeIM	83.2	0.5414(1)	5.3(8)	3.7	3.4/3.4[a]
Au5YCeIM	76.1	0.5414(1)	7.2(6)	4.5	2.4
Au7.5YCeIM	55.9	0.5413(2)	6.7(15)	2.8	3.5/3.4[a]
Au1YCeCP	90.0	0.5417(1)	8.1(15)	6.0	3.2
Au2.5YCeCP	88.7	0.5413(1)	5.1(8)	5.3	2.2/2.3[a]
Au5YCeCP	82.4	0.5419(5)	4.3(8)	5.5	2.4
Au7.5YCeCP	60.1	0.5414(3)	4.7(9)	4.7	2.5[b]/2.2[a,b]

* The numbers in brackets give statistical error of the last figure of the number. It is presented only for numbers determined by statistical fit and the error is determined as the error of regression.
[a] Spent catalyst.
[b] Some gold particles bigger than 10 nm were also observed.

and Au7.5YCeIM fresh and spent catalysts. Brighter points in the HAADF images show gold nanoparticles. From this type of images, reliable particle size measurements were made in order to obtain the size distribution histograms (Fig. 5) and the average size of gold particles (given in Table 1). The results showed small gold particles with average particles size in the range 2.1–3.5 nm for the fresh and also for the used gold catalysts (analyses for spent catalysts with 2.5 and 7.5 dopant amount, prepared by both CP and IM methods, were performed). For theAu7.5YCeCP catalyst, the quantity of highly dispersed gold was accompanied by rarely distributed particles bigger than 10 nm.

Supplementary, the measurements of the interplanar distances in selected HRTEM images of Au1YCeIM, Au2.5YCeIM and Au7.5YCeIM catalysts (Fig. 6A–C, correspondingly) were carried out. The marked zones (Fig. 6) correspond to Y_2O_3 crystals because the crystallographic planes indicated in the respective Fast

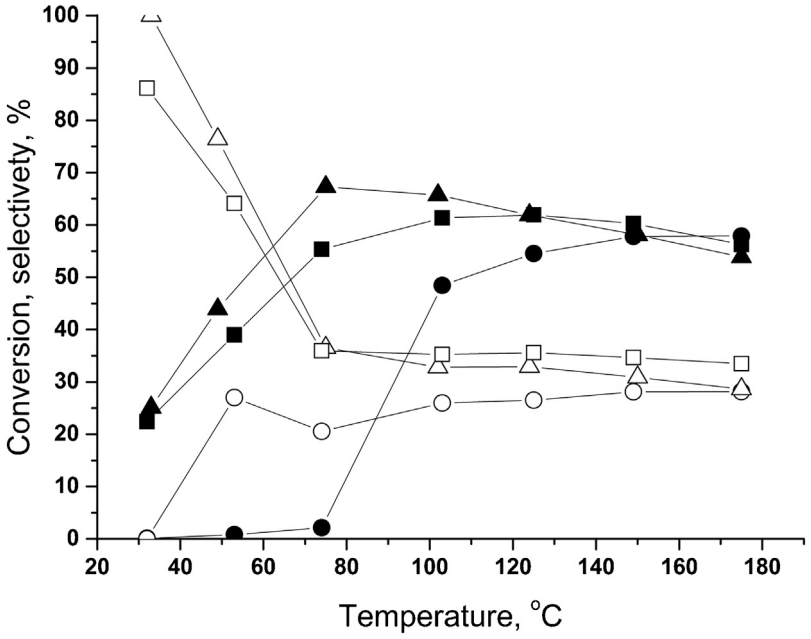

Fig. 2. PROX over Au2.5YCeIM catalyst using feed composition 50% H_2 + 1% CO + 1% O_2 + 10% CO_2 + 10% H_2O (He as balance): (-▲-)—CO conversion and (-Δ-)—selectivity, as well as over Au2.5YCeCP catalyst: (-●-)—CO conversion and (-○-)—selectivity.

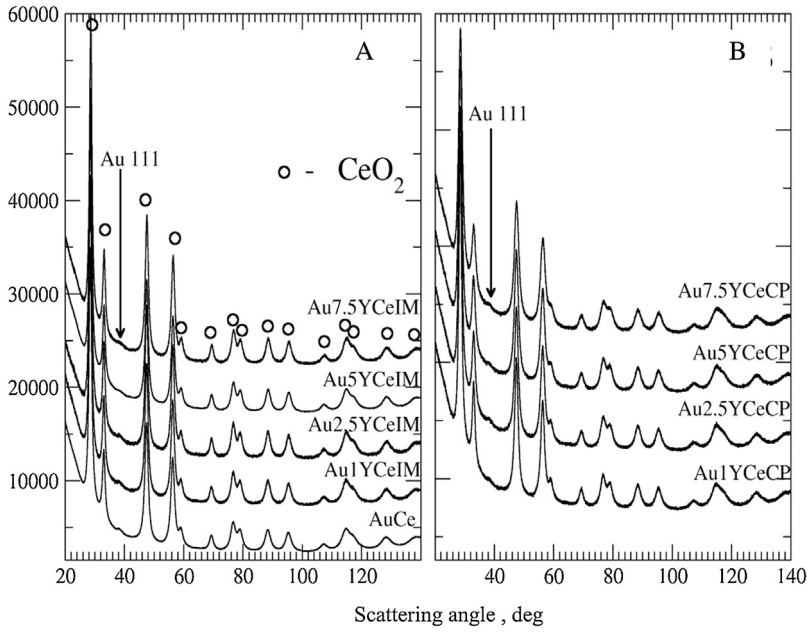

Fig. 3. XRD patterns of the studied gold catalysts: (A) gold catalysts on IM prepared supports and (B) gold catalysts on CP prepared supports.

Fourier transforms (FFT) images correspond to the lattice distances reported in JCPDS data file 88-1040. These observations showed that the use of the IM method results in covering of some ceria particles by a Y_2O_3 phase even in the case of 1 wt.% dopant amount, where some Y_2O_3 crystals can be scarcely distinguished.

The chemical state of gold and Ce in the selected (Au2.5YCeIM and Au2.5YCeCP) fresh and *in situ* pre-reduced catalysts (following the conditions of H_2 pretreatment before PROX) was evaluated by X-ray photoelectron spectroscopy. The experimental and fitted Au 4f XP spectra are compared in Fig. 7 and the corresponding data of Au $4f_{7/2}$ are shown in Table 3. For both fresh catalysts, in complement to metallic gold (Au°) with binding energy (BE) of Au $4f_{7/2}$ peaks 84.1 and 84.2 eV, positively charged Au species with higher BE were detected as well. After the reductive treatment of Au2.5YCeIM and Au2.5YCeCP catalysts, Au $4f_{7/2}$ peaks located at BE 84.3 and correspondingly 84.4 eV were detected. In the case

Table 2
Experimental HC for ceria surface layers reduction of the studied gold catalysts.

Catalysts	HC (mmol/g)	
	CP	IM
AuCe	0.5	
Au1YCe	0.7	0.6
Au2.5YCe	0.8	0.6
Au5YCe	0.8	0.6
Au7.5YCe	0.8	0.6

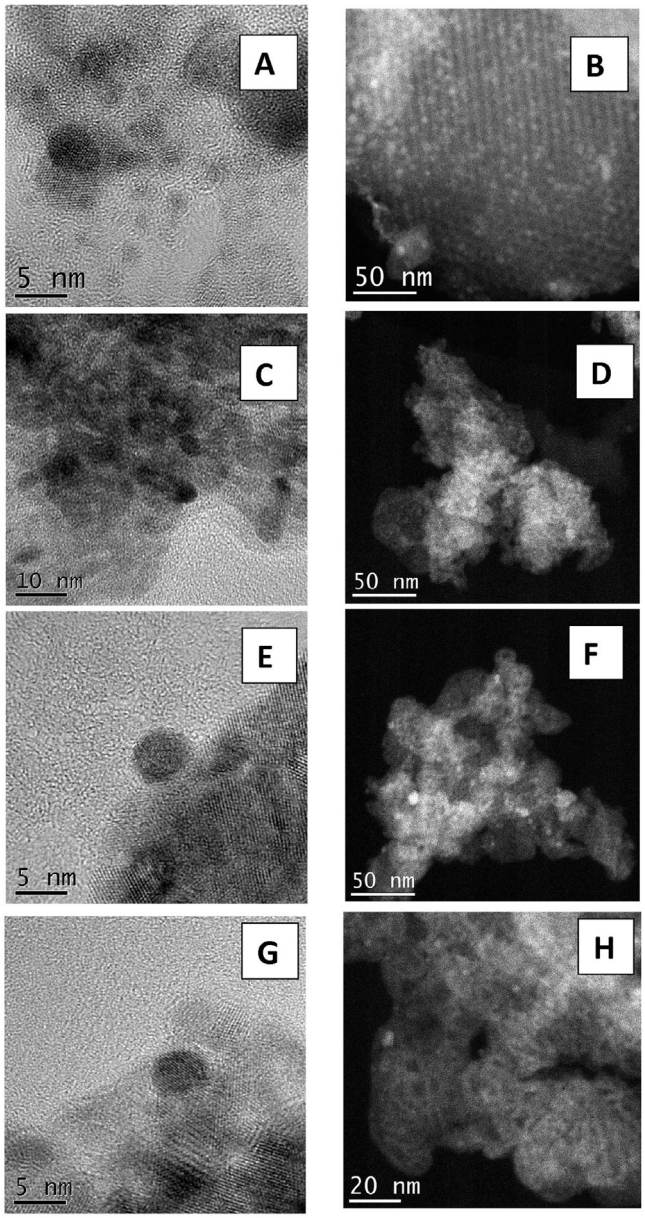

Fig. 4. (A) HRTEM and (B) HAADF images of Au2.5YCeIM fresh catalyst; (C) HRTEM and (D) HAADF images of Au2.5YCeIM used catalyst; (E) HRTEM and (F) HAADF images of Au7.5YCeIM fresh catalyst; (G) HRTEM and (H) HAADF images of Au7.5YCeIM used catalyst.

Table 3
XPS data of the studied samples.

Catalyst	Au $4f_{7/2}$		Ce $3d_{5/2}$ (Ce^{3+})	
	BE (eV)	area (%)	BE (eV)	at. (%)
Au2.5YCeIM as received	84.1 85.6	72.8 27.2	880.1 883.8	29.8
Au2.5YCeIM reduced	84.2 86.2	95.2 4.8	881.2 883.2	34.9
Au2.5YCeCP as received	84.3 85.8	83.0 17.0	880.3 884.9	17.7
Au2.5YCeCP reduced	84.4	100	881.0 887.4	31.5

of Au2.5YCeIM sample a small contribution of XP peak with BE of 85.8 eV has to be taken also in consideration. According to the literature data, Au $4f_{7/2}$ photoelectron peak located at around 84.4 eV is related to Au°, while BE = 85.8 BE eV can be assigned to Au^{1+} species [25 and references therein].

In all cases both Ce^{4+} and Ce^{3+} cations were observed, as expected the concentration of Ce^{3+} was higher in the reduced samples (Table 3).

Raman spectroscopy was used for characterizing the defects induced by Y_2O_3—doping in the ceria structure. Ceria has a fluorite—type cubic matrix (space group *Fm3m* (O_h^5)) with an exceptionally simple vibrational structure with one Raman active mode (F_{2g}), typically (*i.e.*, at room temperature) observed at 465 cm^{-1} that is due to symmetric breathing of O atoms surrounding each Ce^{4+}. The F_{2g} band characteristics (width, position) are extremely dependent on the disorder induced in the oxygen ion sub-lattice of the oxide. Therefore, any distortion or oxygen atom displacement is (due to the high O polarisability) expected to create a response in the Raman spectrum. Inherent punctual defects are known to occur even in pure CeO_2, as a result of which, bands that would otherwise be Raman inactive appear due to local lowering of symmetry. Such punctual defects are manifested by weak bands (leaking from relaxation of symmetry selection rules for

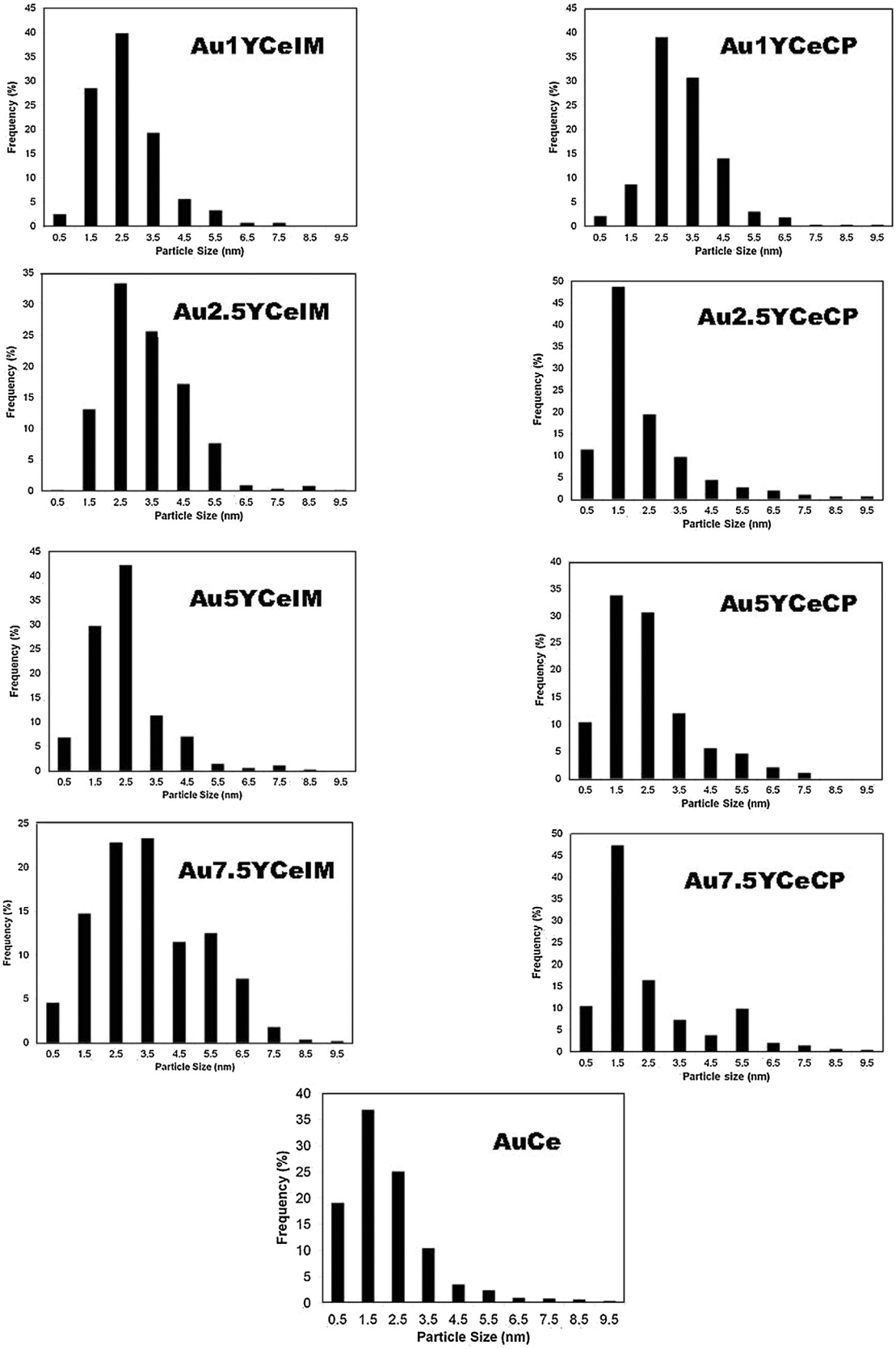

Fig. 5. Size distribution histograms of gold particles for the studied catalysts.

cubic CeO_2) at *e.g.*, *ca.* 600 cm^{-1} (longitudinal optical (LO) mode) and at 250–275 cm^{-1} (zone center transverse optical (TO) mode) that would otherwise both be Raman inactive [26]. The component at 600 cm^{-1} has initially been assigned to intrinsic O vacancies in ceria due to its eventual non-stoichiometric composition (presence of Ce^{3+} in the lattice) [27,28]. Additionally, the creation of O

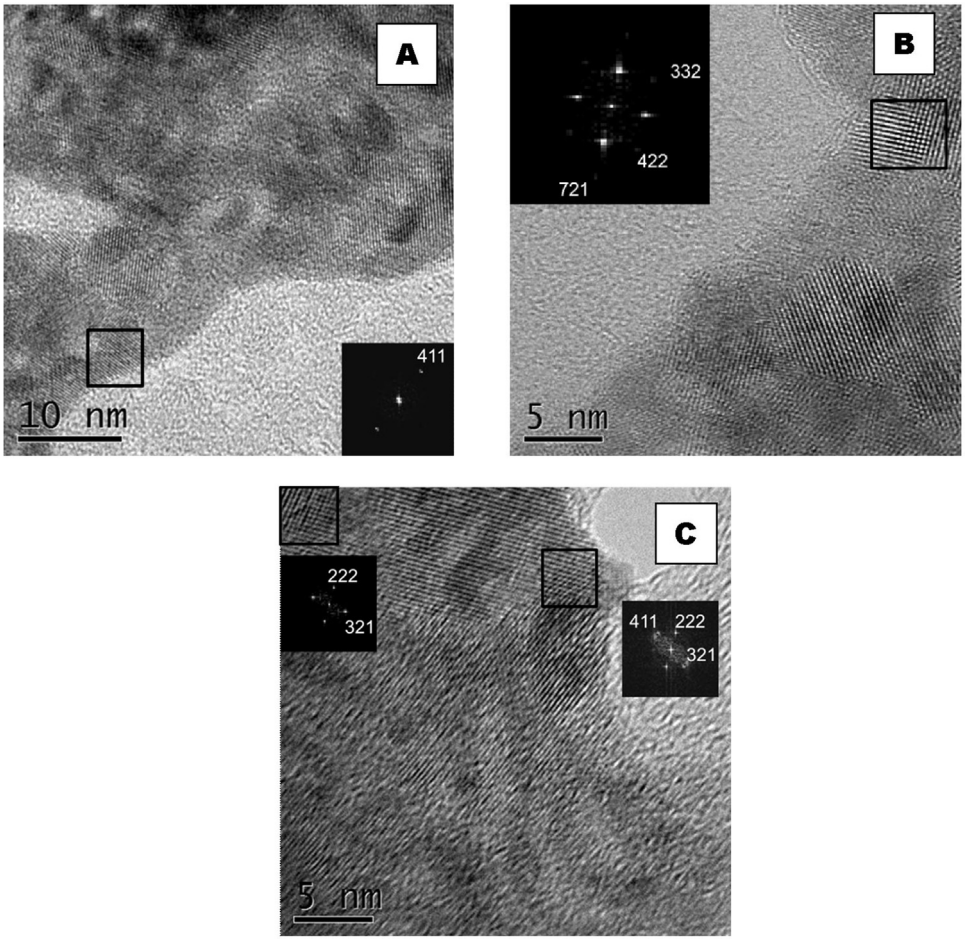

Fig. 6. Selected HRTEM with the corresponding FFT images of (A) Au1YCeIM, (B) Au2.5YCeIM and (C) Au7.5YCeIM catalysts.

vacancies in ceria has been proposed to take place by means of a vacancy-interstitial-O-defect mechanism proposed by Mamontov et al. [29]. Such interstitial O atoms originate from O relocation from the center of tetrahedral cation sub-lattices to the—ideally—empty interior of octahedral cation sub-lattices. Notably, the O vacancies left in the tetrahedral sites are charge—balanced by the O atoms in the interstitial sites [29]. Such interstitial O atoms may also be more labile under reducing atmosphere.

Moreover, when CeO_2 is doped by a trivalent metal oxide, *e.g.*, Y_2O_3, additional O vacancies are generated in the O—sub-lattice in order to compensate the effective negative charge induced by the $Ce^{4+} \rightarrow Y^{3+}$ substitution. Thus, additional distortion is induced in the cubic matrix of the resulting Y_2O_3—CeO_2 mixed oxide. It is noteworthy that although O displacements from ideal (fluorite) positions and local perturbations in the cation coordination number (*e.g.*, from CN = 8 to CN = 7) are expected, no significant lattice expansion is envisaged because of the proximity of the pertinent cation ionic radii (0.97 Å for Ce^{4+} and 1.02 Å for Y^{3+} in eight-fold coordination). A band at *ca.* 560 cm^{-1} is typically the fingerprint of a defect arising from O vacancies generated by the insertion of rare earth RE^{3+} ions in the CeO_2 structure [27,28,30].

Fig. 8 shows the Raman spectra obtained at 200 °C under flowing 20% O_2/He for the doped Y_2O_3—CeO_2 supports made by the IM (Fig. 8A) and CP (Fig. 8B) methods. The Raman spectra of pure CeO_2 supports are included as reference. An intense band at *ca.* 460 cm^{-1}, ascribed to the Raman active F_{2g} mode (the single allowed Raman mode in metal oxides with a fluorite structure) was observed in all spectra. Though the dopant amount increased from 1 to 7.5 wt.%, no shift of the F_{2g} mode was observed, due to the proximity in the ionic radii of Ce^{4+} and Y^{3+}as described above. However, as shown in Fig. 9A, the full width at half maximum (FWHM) was systematically higher for the supports prepared by CP as compared to the respective samples made by the IM method. Moreover (Fig. 9A), the F_{2g} FWHM appears to increase with increasing Y-dopant amount for the CP supports, whereas no variation is observed for the IM prepared supports with increasing Y-doping (Fig. 9A). The FWHM of the F_{2g} mode is largely affected by the defects in the cubic ceria lattice. The average size of ceria particles did not differ significantly for the corresponding samples prepared by IM and CP. Therefore, the differences in FWHM of the F_{2g} mode is to be ascribed to variations in the extent of defects, distortion and symmetry lowering of the cubic matrix resulting by the extent of Y^{3+} incorporation into the ceria cubic matrix that appear to be much higher for the supports made by CP preparation method. A band at *ca.* 560 cm^{-1} (not present in the Raman spectra of pure CeO_2) is clearly visible in the spectra of the doped supports (see insets Fig. 8). Notably, the 560 cm^{-1} band intensity increases (*e.g.* relative to its 600 cm^{-1} counterpart) with increasing Y—doping and moreover its intensity is much stronger for the CP supports compared to the respective relative intensity measured for the IM supports. As mentioned above the *ca.* 600 cm^{-1} component can be assigned due to vacancy-interstitial-O defects (present as inherent defects also in pure ceria and/or generated as a result of lattice deformations) whereas the 560 cm^{-1} component is due to heterovalent dopant-induced O vacancies/defects. The convolution of the 560 and 600 cm^{-1} components is referred as D (defect) band. A comparison of Y-doped supports synthesized by the IM and CP methods showed that the D band intensity is significantly stronger for the CP supports,

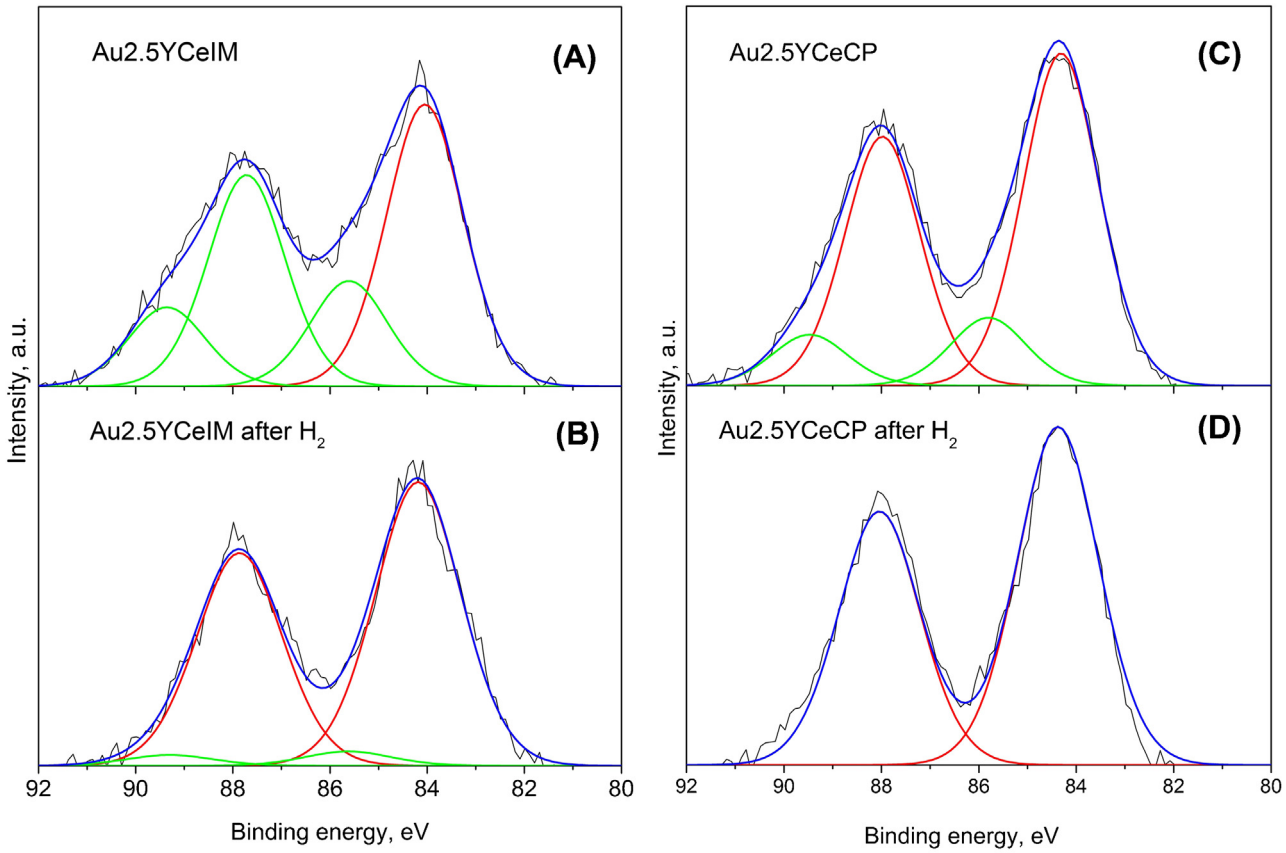

Fig. 7. Experimental and fitted Au 4f XP spectra of Au2.5YCeIM catalyst: (A) as received and (B) after *in situ* H_2 treatment; and of Au2.5YCeCP catalyst: (C) as received and (D) after *in situ* H_2 treatment.

compared to their IM counterparts. A quantitative exploitation of the relative normalized Raman intensities of the D and F_{2g} bands is quite illustrative (Fig. 9B). The plot in Fig. 9B shows the dependence of the $I_D/I_{F_{2g}}$ ratio on the extent of Y-doping for both series of supports. It is evident that the $I_D/I_{F_{2g}}$ ratio is higher for the CP supports and has, furthermore, a tendency to increase with Y-doping, contrary to the case of IM supports where a "saturation"-like behavior is depicted. This behavior is fingerprinting a progressive Y^{3+} incorporation into the CeO_2 cubic matrix with increasing Y-doping for the CP supports. To the contrary, the $I_D/I_{F_{2g}}$ *vs.* Y-doping behavior for the IM supports is suggestive of Y_2O_3 segregation, probably in the form of some Y_2O_3 phase covering ceria as described above (Fig. 6).

At this point it is of relevance to provide evidence showing that the ~600 cm^{-1} component of the D band is indeed due to O atoms in interstitial sites (as described) that can become available under reducing conditions as presumed above. In order to make the detachment of the aforementioned O atoms feasible and detectable by Raman spectroscopy, the temperature of the *in situ* Raman cell was raised to 480 °C and following 1 h of treatment under flowing 20% O_2/He gas, the Raman spectrum was recorded. Subsequently, the inlet gas stream was *switched* to 5%H_2/He, the sample was subjected to hydrogen containing flowing gas for 2 h and the Raman spectrum was recorded at 480 °C under flowing 5% H_2/He. The results are shown in Fig. 10, where (for the interest of space) only results pertaining to the high doped samples 7.5YCeCP and 7.5YCeIM are illustrated. Notably, in order to be able to disentangle the changes caused in the vibrational lines by temperature (thermal effects) from changes caused by alterations of local species and/or modifications in structure, the so-called *reduced representation* of the Raman spectrum is used in Fig. 10. The reinstatement of the oxidized state for the 7.5YCeCP and 7.5YCeIM supports was confirmed by re-subjecting the samples to flowing 20% O_2/He at 480 °C (after they have been treated under 5% H_2/He) and recording a final Raman spectrum under oxidizing conditions (not shown).

The reducibility of gold catalysts was studied by means of TPR. The TPR profiles at the temperature interval up to 250 °C are illustrated in Fig. 11(A and B in the case of supports prepared by IM and CP, correspondingly). It is well known that in this temperature range the surface layers of ceria undergo reduction, enhanced by nanosized gold. The peaks of samples containing Y are apparently double consisting of low and high temperature contributions. The latter is in the range of pure ceria surface layers reduction (see TPR of AuCe). The former can be assigned to the removal of most mobile oxygen species caused by Y-modification as the effect of gold with similar dispersion has to be the same for all catalysts. A comparison of the T_{max} of the TPR profiles shows that there are no substantial differences resulting from the preparation method of ceria supports and from the Y-dopant amount. Barely a tendency of slightly lower T_{max} < 100 °C in the case of IM supports is visible (excluding Au7.5YCeIM with T_{max} > 100 °C) as compared to the CP supports. In Table 2 are given the calculated values of hydrogen consumption (HC). The lowest HC exhibited AuCe catalyst in agreement to the opinion that the Y^{3+}—induced ceria defects could promote the reducibility not only dynamically but also energetically [31]. The HC of gold catalysts on CP supports is higher than that on supports prepared by IM. Based on the Au content (3 wt.%) in the present catalysts, the hydrogen consumption due to the contribution of possibly positively charged gold is negligible with respect to the ceria reduction.

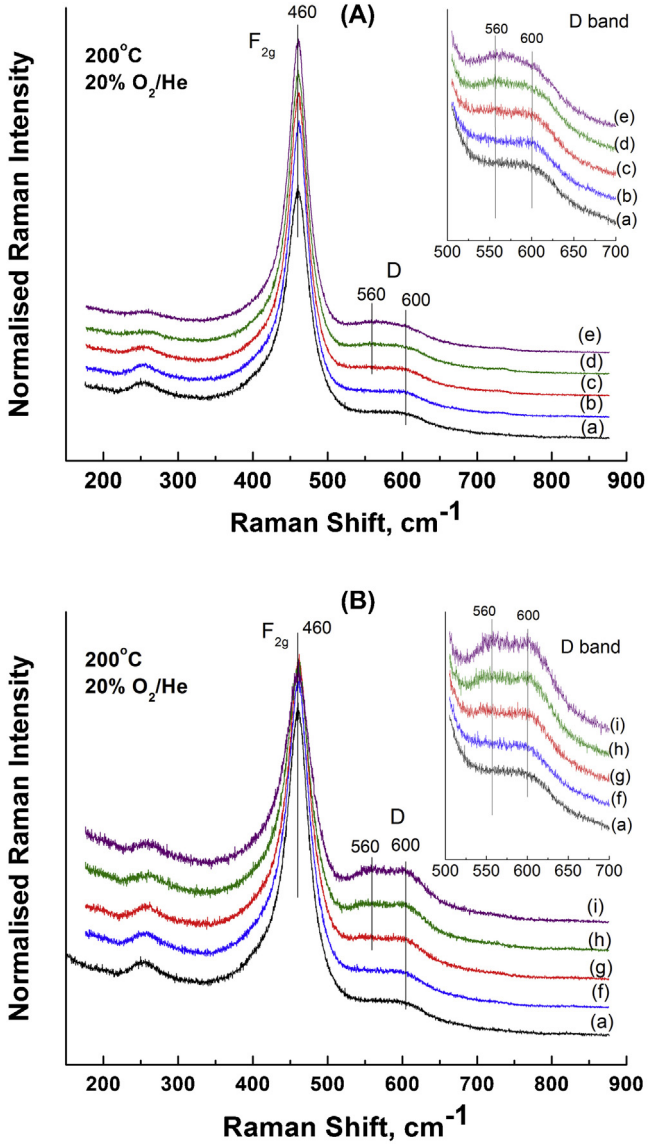

Fig. 8. Raman spectra of Y-doped ceria supports obtained under flowing 20% O_2/He at 200 °C. (A) *x*YCeIM supports: (a) CeO_2, (b) 1YCeIM, (c) 2.5YCeIM, (d) 5YCeIM, (e) 7.5YCeIM. (B) *x*YCeCP supports: (a) CeO_2, (f) 1YCeCP, (g) 2.5YCeCP, (h) 5YCeCP, (i) 7.5YCeCP. Laser wavelength, 491.5 nm; spectral slit width, 6 cm^{-1}; time constant, 0.6 s; laser power, 40 mW.

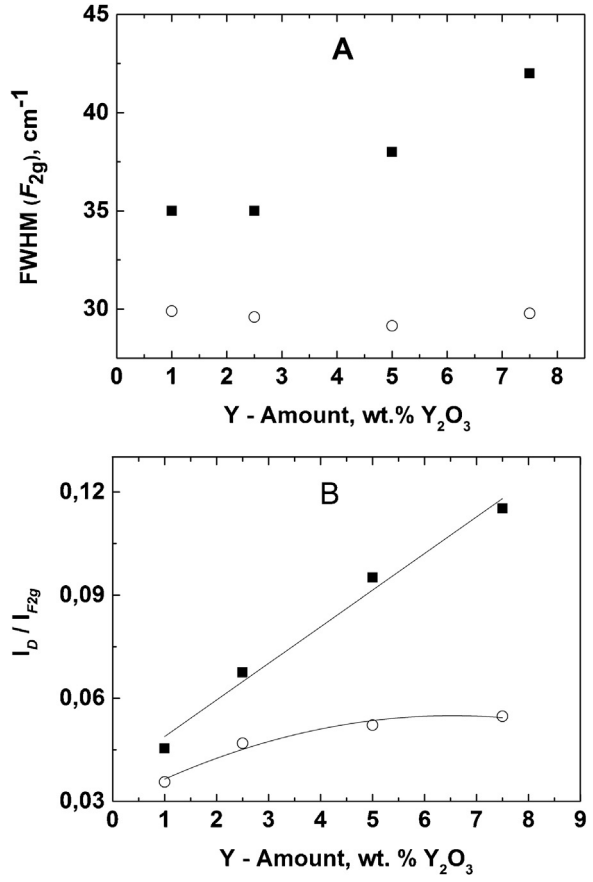

Fig. 9. Dependence of (A) the FWHM (cm^{-1}) and (B) the relative concentration of oxygen vacancies (expressed as $I_D/I_{F_{2g}}$ ratio) on the Y-dopant amount for the supports prepared by the CP method (filled squares) and by the IM method (open circles).

4. Discussion

Various mechanisms of PROX in the presence of gold on reducible and on non reducible oxides have been widely discussed in the literature [2 and references therein]. Evidence substantiating the predominant operation of the gold-assisted Mars–van Krevelen mechanism has been given in the case of reducible supports [32–34].

Consentient opinions exist about CO activation on gold. The gold dispersion is a key factor and it has been established that relatively less CO adsorbs on larger Au particles [35]. However, CO oxidation is a structure-sensitive reaction and an optimum in particle diameters exists (over Au/TiO_2 it ranged from 2.5 to 3.0 nm [36]): not only larger but also the smaller gold particles exhibit less activity. The origin of these observations was explained by quantum size effects with respect to the thickness of the Au particles [36,37]. The role of gold dispersion is even more complicated for PROX because the presence of small particles enhances the undesired H_2 oxidation. Gold dispersion depends on the method of synthesis as well as on the nature and the amount of dopant in ceria-based supports. In the present case the average size of gold for Au on bare ceria was 2.1 nm and in the case of light Y-doping, gold particles with also relatively small average size (estimated in the 2.2–3.5 nm range by HRTEM, with some differences in the distribution, as illustrated in Fig. 5) were obtained both by the IM and CP preparation methods. The generally bigger gold crystallite sizes evaluated by XRD could be due to the contribution of some rarely distributed bigger Au crystallites, not being sampled by the TEM analyses performed on a limited number of particles. The slight differences in particle sizes could account for the similarity in the PROX behavior at 80–120 °C. Likewise the higher CO conversion over Au1YCeIM, Au2.5YCeIM and Au5YCeIM catalysts and the relatively lower activity in the case of AuCe and 7.5 wt.% Y doped samples at ~40 °C cannot be attributed to the dispersion of gold.

There is still no a general agreement about the oxidation state of gold in active supported gold catalysts for CO oxidation. Some authors have considered the important role of positively charged gold [25,38], but other have shown that the metallic Au nanoparticles could play a key role for CO activation [39,40]. In a very recent study Hernández et al. [41] have suggested that the activity loss in PROX is connected to the fast reduction of Au species to metallic state, however it is not unambiguously because of the observed sintering process of Au nanoparticles during the reaction. The results obtained for the gold catalysts here tested showed better PROX performance using reductive pretreatment. Mainly gold in metallic state after H_2 treatment of selected samples was evidenced by *in situ* XPS measurements. On this basis it could be concluded that

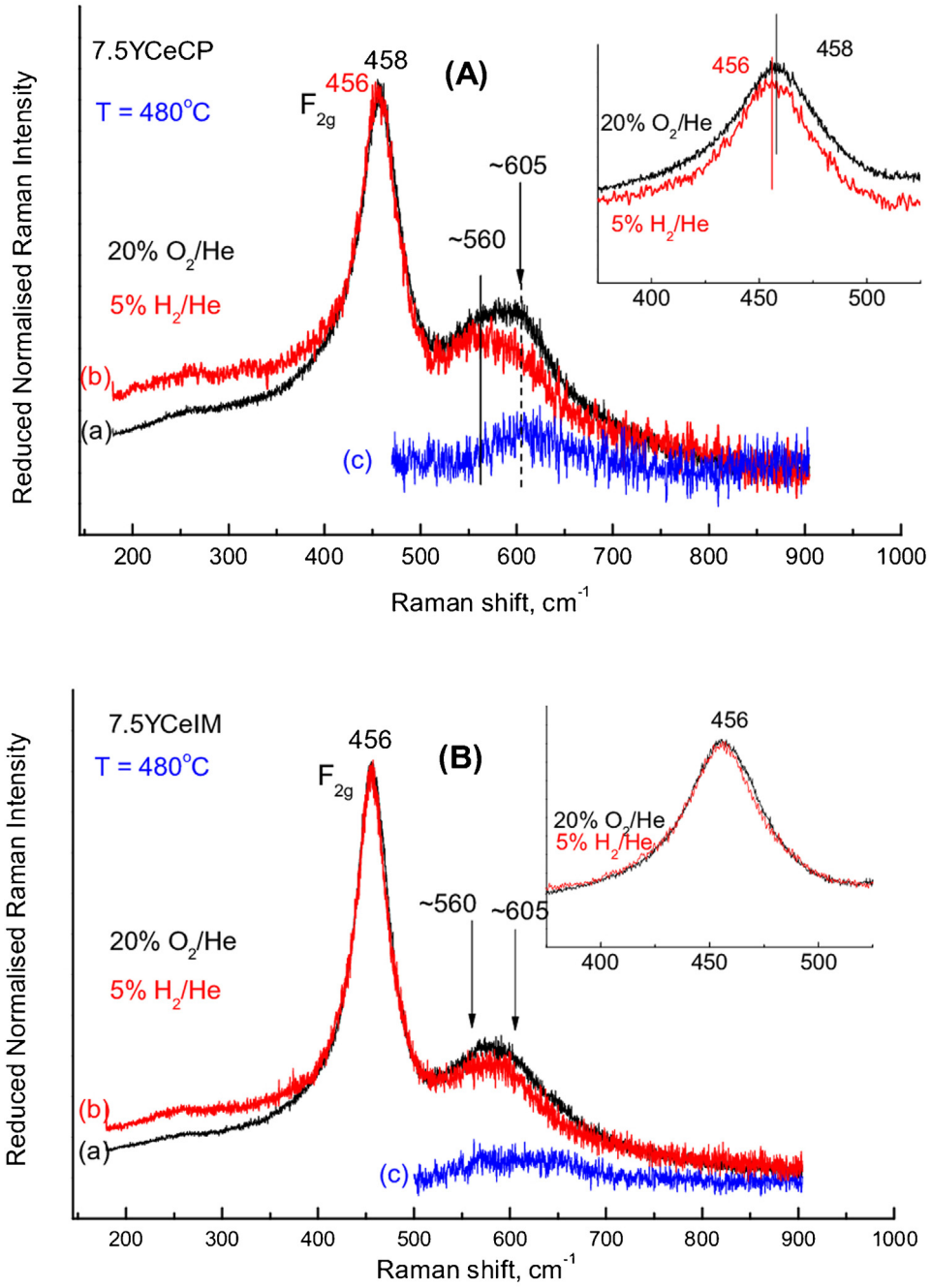

Fig. 10. Sequential *in situ* reduced normalized Raman spectra obtained for 7.5YCeCP (A) and 7.5YCeIM (B) at 480 °C under (a) 20% O_2/He and (b) 5% H_2/He; the trace (c) is obtained by subtracting the spectrum obtained under H_2 from the corresponding spectrum obtained under O_2. Recording parameters: see Fig. 8 caption.

metallic gold particles were favorable to promote PROX reaction. It has to be considered that the role of gold is not only for CO activation but also for the enhancement of the redox properties of ceria supports [42], beneficial for the lattice oxygen supplying. The PROX process is more complicate than CO oxidation and the effect of gold on the competitive undesired H_2 oxidation has to be also taken into account.

Beside its dependence on gold particles, the catalytic activity in CO oxidation is influenced by the active oxygen supplying as well. Concerning ceria as a support, Liotta et al. [43] have concluded that the Mars–van Krevelen mechanism, with gold-enhanced lattice oxygen participation in the reaction, has a significant role in addition to the gold perimeter effects. Accordingly, the support plays a key role in PROX and a summary of results for PROX over gold catalysts presented in [2 and references therein] concludes that the size of the support particles (especially Fe_2O_3 and CeO_2) exerts a significant influence on the catalytic performance. The XRD data in the present study showed nanosized ceria crystallites below 10 nm with small differences in the average size for all studied catalysts.

The ceria supports redox features are very important for enhanced delivery of oxygen. Doped ceria may accommodate a high number of oxygen vacancies by the substitution of elements on the cation sub-lattice. This gives high oxygen ion conductivity and simultaneously, high oxygen supply properties are achieved. These features are influenced not only by the type but also by the amount of dopant. It is known that by increasing the dopant concentration ordered structures (nanodomains) emerge in doped ceria [12,44]. When the oxygen vacancies are ordered in nanodomains [45], they

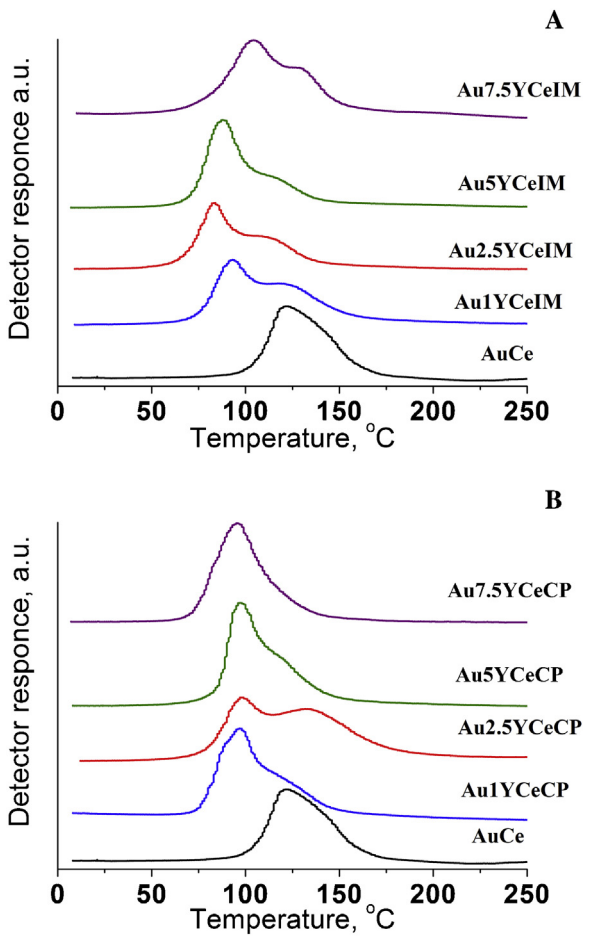

Fig. 11. LT TPR profiles of the studied gold catalysts on supports prepared by (A) IM and (B) CP method.

cannot move freely and this is directly related to the limited mobility of oxygen in ceria lattice. Both the density and the size of nanodomains increase by raising the concentration of dopant. After studying the microstructure evolution of $Y_xCe_{1-x}O_{2-\delta}$ ($x = 0.1$, 0.15, 0.2 0.25) by impedance spectroscopy and TEM technique, Yan et al. [14 and references therein] suggested that a blocking effect for the segregation of nanodomains occurs when the doping level is lower than 15 at.%. Oxygen vacancy ordering was deduced based on neutron diffraction experiments and reverse Monte Carlo modeling of $Ce_{1-x}Y_xO_{2-x/2}$ by Burbano et al. [13]. The presence of a maximum in the ionic conductivity as a function of x was also explained by the vacancy–vacancy interactions becoming dominant at high values of *x*. The authors proposed that the evidenced preference of vacancies association with Y cations is rather weak and at the temperature range of their study (600–800 °C) [46,47], such a weak ordering tendency is washed out by entropic effects. They claimed that the vacancy ordering tendencies in fluorite-structured materials are very similar and that the most important effect is the tendency for vacancies to order along the (1 1 1) direction, which is little influenced by either the dopant or the host cation species. Regardless the type of vacancy ordering, it was concluded [13] that their interactions suppress the conductivity of $Ce_{1-x}Y_xO_{2-x/2}$. Considering the aforementioned evidence for vacancy ordering in the case of heavy Y-doping, in the present study the variation of Y at.% was limited to 11 at.% (*i.e.*, up to 7.5 wt.% Y_2O_3). The Raman results (Figs. 7 and 8) show that a higher extent of defects associated with (i) O vacancies resulting from $Y^{3+} \rightarrow Ce^{4+}$ substitution ("defect" band at *ca.* 560 cm^{-1}) and (ii) interstitial O defects/vacancies ("defect" band at *ca.* 600 cm^{-1}) is evidenced for the supports prepared by CP compared to the corresponding supports made by the IM method. This is expressed quantitatively by exploiting the relative normalized Raman intensities and plotting the $I_D/I_{F_{2g}}$ ratio for the various support samples *vs.* the extent of doping (Fig. 9B). The I_D intensity embodies contributions from both "defect" bands (*i.e.*, at *ca.* 560 and *ca.* 600 cm^{-1}). Moreover (see insets Fig. 8) the *ca.* 600 cm^{-1} "defect" band (associated with interstitial defects/vacancies of the cubic matrix) is relatively stronger from its *ca.* 560 cm^{-1} counterpart for the CP samples. Additionally, a plot of the FWHM of the F_{2g} band for all samples (Fig. 9A) shows that the FWHM is significantly larger for the CP supports and has a clear tendency to increase with increasing extent of Y-doping. This tendency indicates a higher extent of Y^{3+} incorporation into the ceria matrix for the CP supports and is in line with the observation of Y_2O_3 micro-phases for the IM supports, as evidenced by HRTEM (Fig. 6). Seen from another angle, the IM supports exhibit a less extensive creation of defects caused by vacancies and interstitials, in line with the narrow FWHM measured for the F_{2g} band (Figs. 8A and 9 A) and lower $I_D/I_{F_{2g}}$ ratios compared to the corresponding CP-prepared supports (Fig. 9B).

Moreover, the Raman spectra illustrated in Fig. 10 show that the ~600 cm^{-1} component of the D-band, which is more intense for the oxidized state of the 7.5YCeCP sample (compared to its 7.5YCeIM counterpart, see also Fig. 8) is the only band undergoing intensity decrease upon exposure of the sample to H_2(g) containing atmosphere. This is clearly ascribed to removal of available oxygens from the interstitial sites (see above). The traces marked by (c) in Fig. 10 are obtained after subtracting the spectra obtained under H_2(g) from the corresponding spectra obtained under O_2(g) and therefore represent the fingerprint of the *detached* oxygens, *i.e.*, due to vibrational metal-oxygen modes within the anionic (oxygen) sublattice that involve such mobile (detachable) oxygen atoms that can be delivered under suitable conditions. The subtraction reveals that the actual position of the band due to the aforementioned mode is at ~605 cm^{-1}. A treatment under H_2(g) at elevated temperature results in a detachment of such (available) oxygens and causes a lowering in the intensity of this band. This is, to the best of our knowledge, the first report of pertinent evidence in the literature of ceria based mixed metal oxides.

The larger extent of reduction in the case of the 7.5YCeCP support results in a slight red shift of the main F_{2g} band of the cubic matrix (from 458 to 456 cm^{-1}, see inset Fig. 10A). This shift is fully accounted for by a slight expansion of the lattice caused by the partial reduction of Ce^{4+} (i.r. of 0.97 Å in 8-fold coordination) to Ce^{3+} (i.r. of 1.14 Å in 8-fold coordination). No such shift is observed for the 7.5CeIM sample upon exposure to H_2(g) containing gas (see inset Fig. 10B).

The similarity in the range 80–120 °C of PROX behavior over AuCe and over Au catalysts both on IM and CP prepared ligthly Y-doped ceria supports should be explained by the likeness in the size of gold particles responsible for CO activation and similar availability of active oxygen supplying. It is worth to notice that the progressive Y^{3+} incorporation and defects formation into the CeO_2 cubic matrix with increasing Y-doping for the CP supports reflected on the higher HC consumption during TPR of gold catalysts on these supports (Table 2), however it does not result in a corresponding increased order of activities. It can be concluded that the highly mobile surface oxygen has an important role for the PROX activity and therefore appropriate preparation methods for predominant surface modification have to be selected.

In the low temperature interval 40–80 °C, the lowest CO conversion over gold on bare ceria is in agreement with the TPR profile of AuCe—as it was already mentioned, as compared to the Y-facilitated surface ceria reduction, in the case of gold on bare ceria a lack of

the lower temperature part is visible (Fig. 11). However, the higher activities of gold catalysts on IM supports are not in correlation with the quantitative data for HC during the TPR of the studied samples (Table 2): the gold catalysts on the supports prepared by CP showed higher HC but lower CO conversion as compared to the IM method. The Au1YCeIM, Au2.5YCeIM and Au5YCeIM catalysts exhibited very high CO conversion. The eventual explanation could be related to the presence of nanosized Y_2O_3 particles at the surface of modified ceria (bigger particles could be caused by higher Y-concentration). An Y_2O_3 phase was not detected by XRD but very small Y_2O_3 crystals in the case of the IM preparation were proven on the basis of the interplanar distances in selected HRTEM images (Fig. 6). The higher activity registered at such LT could be related to the CO oxidation contribution of the Au/Y_2O_3 nanostructures following the mechanism on inert oxides, where the active oxygen originates mainly *via* direct dissociative adsorption on the gold particles [48]. In accordance to this, Guzman and Corma have established that nanocrystalline Y_2O_3 stabilizes more active species of gold and increases the CO oxidation activity of the gold catalyst [49].

In the recent review of gold catalysts for PROX [2] a typical shape of the curve for CO conversion was illustrated and commented: at the beginning, in the low temperature interval, CO conversion increases but an inflection point exists in the temperature profile, above which a decrease in CO conversion is usually registered. Such shape of the curve is determined by the dual role of hydrogen present in excess. H_2 facilitates CO oxidation at low temperatures. On one hand, this beneficial effect of H_2 on the CO oxidation was mostly related to the prevention of deactivation as the intermediates transformed into stable surface species like carbonates that could be removed by reaction with hydrogen. On the other hand, it could be connected to the participation in the CO oxidation reaction of additional reactive intermediates containing hydroxyl groups [50 and references therein]. In the higher temperature region the role of H_2 was negative because it competes effectively with CO and the process of hydrogen oxidation becomes noticeable. This determines the presence of an inflection point in the temperature profile, above which the boost of the undesired oxidation of hydrogen into water is consequent. The effects were found to be dependent on the nature of the oxide supports [2 and references therein].

In the present case the differences between curve shapes related to the gold catalysts on IM supports containing 1, 2.5 and 5 wt.% dopant and other studied gold catalysts could be explained by their different reactivity at low temperatures: for the first listed supports the CO conversion at ~40 °C is considerably higher but also higher H_2 oxidation activity starting at lower temperatures could be supposed. By this reason the starting temperature for unwanted H_2 oxidation could be about or below 40 °C (making it invisible in the given temperature interval).

It has to be mentioned that the samples with the highest Y doping (7.5 wt.% Y_2O_3, correspondingly, 11 at.% Y) exhibited a relatively lower activity. The explanation could be related to the literature data about surface Y^{3+} dopant enrichment [51] causing local microstructures. In particular, surface domains containing segregated Y cations strongly associated to oxygen vacancies can be formed. Li et al. have commented that the association tendency among defect species depends on the dopant radius. The larger Ce^{3+}cations (radius of 1.14 Å for Ce^{3+} and 1.02 Å for Y^{3+}) tend to favor longer bonds to oxygen vacancies and occupy the second neighbor sites, while Y^{3+} favors the first neighbor sites [52]. The supplying of active oxygen has to be related to redox transfer $Ce^{4+}\leftrightarrow Ce^{3+}$, accompanied by filling and emptying of the adjacent to oxygen vacancies. The surface microstructures of oxygen vacancies around clustered Y^{3+} cations which have stable valence state, will not participate in the redox process, hindering oxygen provision. This could be the reason leading to lower activity in the case of 7.5 wt.% (11 at.%) dopant amount. Similar interpretation was given by Atribak et al. [15] about the lower activity in the soot oxidation over $Ce_{1-x}Y_xO_2$ with high yttrium loading ($x = 0.12$). The authors supposed that yttrium was mainly accumulated at the surface of the particles hindering the participation of cerium in the oxidation reaction.

The unwanted conversion of H_2 caused selectivity toward CO_2 of around 40% for all studied gold catalyst on Y-doped ceria which is higher as compared to gold on bare ceria (see Fig. 1C and D). Besides the main unwanted process of H_2 oxidation, some other undesirable side reactions could take place together with CO oxidation [2]. It can be supposed that the interaction between CO_2 and H_2, *e.g.* reverse WGS reaction is unlikely to proceed at the temperatures of interest for PROX. CO or CO_2 methanation may probably occur, depending on the nature of ceria doping. While not negligible quantities of methane were detected by Ilieva et al. [53] over gold catalysts on Co-doped ceria, no traces were found in the present study.

PROX catalysts for practical application have to be capable of removing trace amounts of CO from excess of humid H_2 containing significant quantities of carbon dioxide because CO_2 and moisture usually present as side products in the reformate stream. Regarding the effect of water on the PROX activity and selectivity different observations have been reported but the prevailing opinion is about a positive influence of water assigned to the hydroxyl group formation, which is necessary for CO oxidation [54,55], or for enhancing the rate of carbonates decomposition *via* thermally less stable bicarbonate species [56 and references therein,57]. The negative effect of CO_2 on the PROX performance over supported gold catalysts was observed by many authors. Luengnaruemitchai et al. [58] have found that the increasing of CO_2 concentration from 2 to 20% at reaction temperature of 107 °C, reduced the PROX activity of Au/CeO_2 catalyst from about 80% to about 20% (without a significant effect on the selectivity). Avgouropoulos et al. [8] have reported the negative effect of CO_2 on activity and selectivity (being more significant for undoped Au/CeO_2). On one hand the reverse water gas shift reaction between CO_2 and H_2 could occur, leading to the CO formation, thereby the target CO conversion cannot be reached. On the other hand the strong negative role of CO_2 could be ascribed to the competitive adsorption of CO_2 and CO. The accumulation of carbonate and carboxylate species blocking the active sites is depended on the nature of the support [59,60] and the acidic supports were found to be more resistant to deactivation by CO_2 than the basic ones [61].

The results for PROX in the presence of CO_2 and water over gold on bare ceria and the gold catalysts containing 2.5 wt.% dopant are illustrated in Fig. 2. It is clearly seen that IM method is more appropriate than the CP one for PROX under realistic conditions: in the range 80–120 °C the drop in CO conversion and selectivity toward CO_2 was not so drastic over Au2.5YCeIM as compared to Au2.5YCeCP sample. The better resistance to CO_2 deactivation of the catalyst on the IM prepared support could be associated with the nanosized Y_2O_3 particles covering CeO_2 grains as it is known by the literature that CeO_2 has stronger basic properties as compared to Y_2O_3 [62]. The Y_2O_3 particles with lower basicity over CeO_2 grains possibly have higher activity interacting with gold than pure CeO_2 or CeO_2 with incorporated Y^{3+}. A better resistance to CO_2 deactivation was also reported for PROX over gold catalysts on IM ceria supports doped with Fe [63] and by Pr [10]. The significantly worst catalytic behavior of Au2.5YCeCP catalyst than that of AuCe could be related to the higher occurrence of defects due to the Ce^{4+}substitution by the heterovalent Y^{3+}. There are literature data showing a correlation between ceria basicity and the number of oxygen defects: ceria surface with fewer oxygen defects is less basic [64 and references therein].

5. Conclusions

The present study shows that during the PROX in the low temperature interval 40–80 °C the CO conversion over Y-containing gold catalysts is higher when compared to gold on pure ceria. The result is well correlated with the appearance of a lower temperature peak in the TPR spectra of Y-modified samples assigned to the removal of very mobile oxygen species. The substantially higher activity observed at this temperature of gold catalysts on IM supports containing 1, 2.5 and 5 wt.% dopant could be related to the contribution of surface Au/Y_2O_3 nanostructures that are formed when using this preparation method.

In the region of fuel cells operating temperatures (80–120 °C) the selectivity of the lightly Y-doped catalysts was larger than Au/CeO_2, however the CO conversion over gold catalysts on bare ceria and lightly Y-doped ceria (1–5 wt.% Y_2O_3) was quite similar regardless the support preparation method. These catalytic results are in accord with the likeness in the size of gold particles responsible for CO activation and the similar availability of active oxygen supplying affected by the presence of Y^{3+}dopant modification. Raman spectroscopy results showed a higher extent of bulk defects, O vacancies and interstitials with increasing Y-doping in the supports made by the CP method. The absence of correlation between conversion and yttrium loading suggests a preferential role played by the surface modification and surface oxygen mobility in PROX. Worth mentioning is the relatively lower activity in the case of the highest (7.5 wt.%) dopant amount explained by the ordering of surface oxygen vacancies around segregated Y^{3+} hindering oxygen supplying.

The effect of supports preparation method is clearly seen under realistic conditions with CO_2 and water added to the gas feed: the catalysts on the IM prepared supports were more active as compared to those on the CP prepared ones. The better resistance to CO_2 deactivation in the former case was explained by the lowering of ceria surface basicity due to the presence of nanosized Y_2O_3, covering ceria grains.

Acknowledgements

The study was performed in the frame of COST Action CM1104. The Bulgarian team is thankful to the National Science Fund of Bulgaria for the financial support through Project E-02/2-2014. R.Z. acknowledges UNAM PAPIIT-105416project and H_2 network of CONACYT for financial support. The Patras team is grateful to The European Regional Development Fund, the Republic of Cyprus, and the Research Promotion Foundation of Cyprus for their financial support through the TEXNOLOΓIA/θEPIS/0311(BE) and TEXNO/0308(BE)/05 projects. P.P. is grateful to European Social Fund within Operating Program: Development of Human Resources (BG051PO001-3.3.06-0050).

References

[1] S. Kandoi, A.A. Gokhale, L.C. Grabow, J.A. Dumesic, M. Mavrikakis, Catal. Lett. 93 (2004) 93–100.
[2] P. Lakshmanan, J.E. Park, E.D. Park, Catal. Surv. Asia 18 (2014) 75–88.
[3] G. Panzera, V. Modafferi, S. Candamano, A. Donato, F. Frusteri, P.L. Antonucci, J. Power Sources 135 (2004) 177–183.
[4] W.L. Deng, J.D. Jesus, H. Saltsburg, M. Flytzani-Stephanopoulos, Appl. Catal. A 291 (2005) 126–135.
[5] F. Arena, P. Famulari, G. Trunfio, G. Bonura, F. Frusteri, L. Spadaro, Appl. Catal. B 66 (2006) 81–91.
[6] G. Avgouropoulos, J. Papavasiliou, T. Tabakova, V. Idakiev, T. Ioannides, J. Chem. Eng. 124 (2006) 41–45.
[7] A. Jain, X. Zhao, S. Kjergaard, S.M. Stagg-Williams, Catal. Lett. 104 (2005) 191–197.
[8] G. Avgouropoulos, M. Manzoli, F. Boccuzzi, T. Tabakova, J. Papavasiliou, T. Ioannides, V. Idakiev, J. Catal. 256 (2008) 237–247.
[9] L. Ilieva, G. Pantaleo, I. Ivanov, R. Zanella, A.M. Venezia, D. Andreeva, Int. J. Hydrogen Energy 34 (2009) 6505–6515.
[10] L. Ilieva, P. Petrova, T. Tabakova, G. Pantaleo, V. Montes, J.W. Sobczak, W. Lisowski, Z. Kaszkur, M. Boutonnet, A.M. Venezia, Fuel 134 (2014) 628–635.
[11] E.O. Jardim, S. Rico-Francés, F. Coloma, E.V. Ramos-Fernández, J. Silvestre-Albero, A. Sepúlveda-Escribano, Appl. Catal. A 487 (2014) 119–129.
[12] D.R. Ou, T. Mori, F. Ye, M. Takahashi, J. Zou, J. Drennan, Acta Mater. 54 (2006) 3737–3746.
[13] M. Burbano, S.T. Norberg, S. Hull, S.G. Eriksson, D. Marrocchelli, P.A. Madden, G.W. Watson, Chem. Mater. 24 (2012) 222–229.
[14] P.F. Yan, T. Mori, A. Suzuki, Y.Y. Wu, G.J. Auchterlonie, J. Zou, J. Drennan, Solid State Ionics 222 (2012) 31–37.
[15] I. Atribak, A. Bueno-López, A. García-García, J. Mol. Catal. A 300 (2009) 103–110.
[16] Y. She, L. Li, Y. Zhan, X. Lin, Q. Zheng, K. Wei, J. Rare Earths 27 (2009) 411–417.
[17] G.K. Williamson, W.H. Hall, Acta Metall. 1 (1953) 22–31.
[18] V.D. Mote, Y. Purushotham, B.N. Dole, J. Theor. Appl. Phys. 6 (2012) 6–28.
[19] M. Romeo, K. Bak, J. El Fallah, F. Le Normand, L. Hilaire, Surf. Interface Anal. 20 (1993) 508–512.
[20] L. Armelao, D. Barecca, G. Bottaro, A. Gasparotto, E. Tondello, Surf. Sci. Spectra 8 (2001) 247–249.
[21] A.Q. Wang, P. Punchaipetch, R.M. Wallace, T.D. Golden, J. Vaccum Sci. Technol. B 21 (2003) 1169–1175.
[22] G. Tsilomelekis, S. Boghosian, Catal. Sci. Technol. 3 (2013) 1869–1888.
[23] N. Kotzev, D. Shopov, J. Catal. 22 (1971) 297–301.
[24] D.A.M. Monti, A. Baiker, J. Catal. 83 (1983) 323–335.
[25] M.P. Casaletto, A. Longo, A. Martorana, A. Prestianni, A.M. Venezia, Surf. Interface Anal. 38 (2006) 215–218.
[26] W.H. Weber, K.C. Hass, J.R. McBride, Phys. Rev. B 48 (1993) 178–185.
[27] J.R. McBride, K.C. Hass, B.D. Poindexter, W.H. Weber, J. Appl. Phys. 76 (1994) 2435–2441.
[28] Z.D. Dohčević-Mitrović, M. Radović, M. Šćepanović, M. Grujić-Brojčin, Z.V. Popović, B. Matović, S. Bošković, Appl. Phys. Lett. 91 (2007) 203118-1–203118-3.
[29] E. Mamontov, T. Egami, R. Brezny, M. Koranne, S. Tyagi, J. Phys. Chem. B 104 (2000) 11110–11116.
[30] W.Y. Hernandez, O.H. Laguna, M.A. Centeno, J.A. Odriozola, J. Sol. State Chem. 26 (2010) 3014–3020.
[31] G. Balducci, M.S. Islam, J. Kaspar, P. Fornasiero, M. Graziani, Chem. Mater. 15 (2003) 3781–3785.
[32] L. Li, A. Wang, B. Qiao, J. Lin, Y. Huang, X. Wang, T. Zhang, J. Catal. 299 (2013) 90–100.
[33] M.J. Kahlich, H.A. Gasteiger, R.J. Behm, J. Catal. 182 (1999) 430–440.
[34] S. Scire, C. Crisafulli, S. Minico, G.G. Condorelli, A.D. Mauro, J. Mol. Catal. A 284 (2008) 24–32.
[35] C.J. Weststrate, A. Resta, R. Westerstrom, E. Lundgren, A. Mikkelsen, J.N. Andersen, Phys. Chem. C 112 (2008) 6900–6906.
[36] M. Valden, X. Lai, D.W. Goodman, Science 281 (1998) 1647–1650.
[37] M.S. Chen, D.W. Goodman, Catal. Today 111 (2006) 22–33.
[38] J.C. Fierro-Gonzalez, J. Guzman, B.C. Gates, Topics Catal. 44 (1–2) (2007) 103–114.
[39] M.S. Chen, D.W. Goodman, Science 306 (2004) 252–255.
[40] D.C. Maeir, D.W. Goodman, J. Am. Chem. Soc. 126 (2004) 1892–1899.
[41] J.A. Hernández, S.A. Gómez, T.A. Zepeda, J.C. Fierro-González, G.A. Fuentes, ACS Catal. 5 (7) (2015) 4003–4012.
[42] D. Andreeva, V. Idakiev, T. Tabakova, L. Ilieva, P. Falaras, A. Bourlinos, A. Travlos, Catal. Today 72 (2002) 51–57.
[43] L.F. Liotta, G. Carlo Di, G. Pantaleo, A.M. Venezia, Catal. Today 158 (2010) 56–62.
[44] F. Ye, T. Mori, D.R. Ou, J. Zou, G. Auchterlonie, J. Drennan, Solid State Ionics 179 (2008) 827–831.
[45] D.R. Ou, T. Mori, F. Ye, J. Zou, G. Auchterlonie, J. Drennan, Phys. Rev. B 77 (2008) 24108.
[46] N. Kim, J.F. Stebbins, Chem. Mater. 19 (2007) 5742–5747.
[47] H. Maekawa, K. Kawata, Y.P. Xiong, N. Sakai, H. Yokokawa, Solid State Ionics 180 (2009) 314–319.
[48] M.M. Schubert, S. Hackenberg, A.C. van Veen, M. Muhler, V. Plzak, R.J. Behm, J. Catal. (2001) 197–213.
[49] J. Guzman, A. Corma, Chem. Commun. 743 (2005) 745.
[50] C. Rossignol, S. Arrii, F. Morfin, L. Piccolo, V. Caps, J.-L. Rousset, J. Catal. 230 (2005) 476–483.
[51] P.G. Harrison, D.A. Creaser, B.A. Wolfindale, K.C. Waugh, M.A. Morris, W.C. Mackrodt, in: T.J. Dines, C.H. Rochester, J. Thomson (Eds.), Catalysis and Surface Characterisation, The Royal Society of Chemistry, Cambridge, 1996, pp. 76–86.
[52] Z.P. Li, T. Mori, F. Ye, D. Ou, G.J. Auchterlonie, J. Zou, J. Drennan, J. Phys. Chem. 116 (2012) 5435–5443.
[53] L. Ilieva, G. Pantaleo, I. Ivanov, A. Maximova, R. Zanella, Z. Kaszkur, A.M. Venezia, D. Andreeva, Catal. Today 158 (2010) 44–55.
[54] M. Haruta, S. Tsubota, T. Kobayashi, H. Kageyama, M.J. Genet, B. Delmon, J. Catal. 144 (1993) 175–192.
[55] G.Y. Wang, H.L. Lian, W.X. Zhang, D.Z. Jiang, T.H. Wu, Kinet. Catal. 43 (2002) 433–442.
[56] M.M. Schubert, A. Venugopal, M.J. Kahlich, V. Plzak, R.J. Behm, J. Catal. 222 (2004) 32–40.

[57] M. Date, M. Okumura, S. Tsubota, M. Haruta, Angew. Chem. Int. Ed. 43 (2004) 2129–2132.
[58] A. Luengnaruemitchai, S. Osuwan, E. Gulari, Int. J. Hydrogen Energy 29 (2004) 429–435.
[59] M.M. Schubert, V. Pizak, J. Garche, R.J. Behm, Catal. Lett. 76 (2001) 143–150.
[60] A. Luengnaruemitchai, D.T.K. Thoa, S. Osuwan, E. Gulari, Int. J. Hydrogen Energy 30 (2005) 981–987.
[61] G.C. Bond, D.T. Thompson, Catal. Rev. Sci. Eng. 41 (1999) 319–388.
[62] K. Tanabe, M. Misono, Y. Ono, H. Hattori, New Solid Acids and Bases: Their Catalytic Properties, SSSC, Elsevier, 1989, p. 18.
[63] L. Ilieva, T. Tabakova, G. Pantaleo, I. Ivanov, R. Zanella, D. Paneva, N. Velinov, J.W. Sobczak, W. Lisowski, G. Avdeev, A.M. Venezia, Appl. Catal. A 467 (2013) 76–90.
[64] A.M. Venezia, L.F. Liotta, G. Pantaleo, A. Longo, in: A. Trovarelli, P. Fornasiero (Eds.), Catalysis by Ceria and Related Materials, 2nd ed., Imperial College Press, London, 2013, pp. 813–833.